

# Burstiness of Interference Pikes in Wireless Networks

Mahin K. Atiq, Udo Schilcher, Xhemal Pengili, Martin Haenggi, *Fellow, IEEE*,  
and Christian Bettstetter, *Senior Member, IEEE*

The temporal dynamics of interference in wireless networks affects their performance but has only been studied for some cases. This article addresses this gap by analyzing high-interference events, called pikes, concluding that they arrive in bursts in many cases. Specifically, we show that in Poisson networks with random access and multipath fading, the pike interarrival time increases with the interference correlation, irrespective of the source of correlation and burstiness of pikes. To demonstrate the applicability of this theory, we conduct a measurement campaign with an automotive user in different commercial 4G cellular networks. The experimental results indicate that interference pikes are bursty in the real world as well.

*Index Terms*—Interference, wireless, burstiness, fading, Poisson networks, temporal dynamics.

## I. INTRODUCTION

**B**URSTINESS is a phenomenon that occurs in many natural and human-made systems, including earthquakes [1; 2], solar flares [3], neural firings [4], human activity patterns [5], emails [6], library loans [7], and in the context of infectious diseases [8]. It means that several events occur within a short period of time followed by a long period of inactivity. The set of successive events is called a *burst*. The opposite of burstiness is when events occur in regular, periodic patterns. Events uniformly distributed at random are between the two extremes: they are neither bursty nor periodic.

In the domain of computer and communication networks, burstiness is relevant for data traffic patterns [9; 10] and channel coding with interleaving [11–13]. Our work studies for the first time the burstiness of *high-interference events* in wireless networks — we call them *pikes*. To do so, we employ measures from the theory of temporal networks and partly identify the cause for bursty arrival of interference pikes in our system models. Preparatory work was presented in [14].

In wireless systems, burst errors occur when communication takes place over slow fading channels, where deep fades let the signal power fall below a sensitivity threshold for a period longer than the bit, symbol, or slot duration, and these errors are counteracted by incorporating the channel characteristics into the design of wireless communications. The channel dynamics is typically characterized by the coherence time, level crossing rate, correlation, and average fade duration [12]. Some examples of fading mitigation techniques include: using the decorrelation distance of a fading channel to determine the antenna placement in multi-antenna systems [15]; using

the coherence time to decide the separation between symbols of a codeword in a channel code (interleaver depth) in order for them to have independent fading [11; 12]; and using the second-order statistics of the fading channel like the level crossing rate to choose symbol and slot durations [11; 16].

In interference-limited scenarios, the problem is reciprocal: the performance is limited by events with high (interference) power rather than low power. Similar to how channel dynamics is exploited, information on interference dynamics can help in the design of robust communication systems. For example, knowledge on the burstiness of the interference pikes can be used for opportunistic interference management techniques, e.g., multiuser diversity [17–19], efficient detectors [20], opportunistic scheduling [21], dynamic resource management [22], and channel coding [23]. Scientific results on interference dynamics include the derivation of expressions for interference correlation and interference coherence time (i.e., the time until the interference correlation becomes very small) [24–27]. However, a comprehensive analysis of the temporal dynamics of interference pikes is missing so far.

The **main contributions** of this article are as follows:

- We formally model the burstiness of interference pikes and employ measures to quantify it. In particular, we use interference pikes and bursts of interference pikes, and we provide means to quantify their dynamics, such as burstiness and memory coefficients, average burst size, and mean interarrival time of pikes.
- We partly identify the causes of burstiness of interference pikes in different scenarios. Such burstiness typically occurs when we have two overlaying factors influencing interference power, where one is fast and the other slowly changing over time.
- We analyze the burstiness for different interference correlation scenarios that differ by the magnitude and the causes of interference correlation.
- We show the existence of interference burstiness in the real world by analyzing the burstiness for interference measured by a vehicular user connected to different commercial 4G cellular networks.

From a methodical point of view, we employ measures from temporal network theory — burstiness, memory, and burst size [28; 29] — to analyze the bursty arrival of interference

This work was supported in part by the Austrian Science Fund (FWF) under Grant P24480-N15 (Dynamics of interference in wireless networks).

Mahin K. Atiq was with the Institute of Networked and Embedded Systems, University of Klagenfurt, Austria. She is now with Silicon Austria Labs GmbH, Linz, Austria (e-mail: mahin.atiq@silicon-austria.com).

Udo Schilcher was with Lakeside Labs GmbH, Klagenfurt, Austria. He is now with the Institute of Networked and Embedded Systems, University of Klagenfurt, Austria (e-mail: udo.schilcher@aau.at).

Xhemal Pengili was with the Institute of Networked and Embedded Systems, University of Klagenfurt, Austria. He is now with Infineon Technologies, Linz, Austria (e-mail: Xhemal.Pengili@infineon.com).

Martin Haenggi is with the Department of Electrical Engineering and the Department of Applied and Computational Mathematics and Statistics, University of Notre Dame, USA (e-mail: mhaenggi@nd.edu).

Christian Bettstetter is with the Institute of Networked and Embedded Systems, University of Klagenfurt, Austria (e-mail: christian.bettstetter@aau.at).

pikes in both simulations and experiments; the simulations are performed in a broad set of network scenarios that incorporate models for node location and mobility, channel, and data traffic. The following **general insights** are gained for our models:

- The mean interarrival time of interference pikes increases with increasing interference correlation, irrespective of the source of correlation and burstiness of pikes.
- The burstiness of pikes seems to be the result of the overlay of fast and slowly changing factors contributing to the overall interference power. In a static scenario, for example, the burstiness is high when the channel varies fast and data traffic varies slowly (or vice versa).
- The burstiness depends on the type of node mobility. Brownian motion seems to foster burstiness compared to straight movement without any change of direction.

In order to prove the existence of burstiness of interference pikes in the real world, we perform an empirical study of the power received by a phone in an automobile in commercial 4G networks in different environments in two European countries. Burstiness is observed in all scenarios measured. It is higher on the freeway than in urban environments. It seems that a combination of high node speed, fast channel variations, and slow traffic lead to such observations.

The rest of the article is organized as follows: Section II addresses related work. Section III presents the network model with modeling assumptions. Section IV formally defines interference pikes and burstiness measures. Section V is the main part: it contains a comprehensive model-based analysis of pikes for different network scenarios. Section VI presents the experimental analysis of pikes in cellular networks. Section VII discusses the results. Finally, Section VIII draws conclusions.

## II. RELATED WORK ON BURSTINESS OF INTERFERENCE

Burstiness of interference has been considered in the literature but with exclusive focus on exploiting rather than defining and quantifying it. Examples include the following: The capacity region of a two-user single-carrier bursty interference channel is addressed without feedback [19; 30] and with feedback [17]. The authors harness the burstiness of interference by decoding an extra message in the absence of interference. The two-user multi-carrier bursty interference channel is categorized [18] (with feedback). A multi-user bursty interference scenario is analyzed in terms of the achievable rate by adapting the transmission probability of users based on the bursty interference state [31]. The work mentioned above considers bursty interference as a quasi-static channel (i.e., the bursts are defined as absence or presence of interfering links for the full duration of the codeword). The ergodic interference channel is analyzed [21; 23], where secure transmissions using opportunistic scheduling are studied for a bursty interference channel [21]. It has also been identified as to when interference burstiness is beneficial in terms of achievable rates [23] and interference mitigation with in-band relays [32]. In addition to these information-theoretic approaches, an adaptive beamforming strategy and a communication rate exploiting the burstiness of interference has been presented [33].

TABLE I: Notations and symbols

Symbol	Definition/explanation
$t$	time index
$x(t)$	node location at slot $t$
$\Phi$	Poisson point process (PPP)
$\lambda$	PPP intensity
$v$	mean node speed (m/slot)
$d$	message duration (slots)
$\mu$	average fraction of nodes transmitting
$\ell_x$	path loss
$\alpha$	path loss exponent
$g$	fading gain
$m$	Nakagami fading parameter
$c$	channel coherence time (slots)
$I(t)$	interference power in slot $t$ (mW)
$\theta$	interference threshold (mW)
$\xi$	scaling parameter for interference threshold
$\tau_{\mathcal{P}}$	pike duration (slots)
$\tau_{\mathcal{V}}$	valley duration (slots)
$\beta$	burst size (slots)
$\delta$	burst size threshold (slots)
$B$	burstiness
$M$	memory coefficient
$\tau$	pike interarrival time (slots)

All of this work models the interference either as being constant for the whole duration of a codeword (quasi-static) or as a memoryless block-i.i.d. Bernoulli random variable that stays constant for the duration of multiple symbols (ergodic). Thus, the interference correlation is not considered. The interference burstiness is defined as the presence or absence of interfering links. The related work focuses on traffic as the sole reason for the occurrence of interference bursts.

An optimal maximum a-posteriori symbol detection method for bursty external interference is presented in [20]. Although the total received interference is as a random process with memory, the interference correlation is not used to analyze the interference burstiness. Additionally, the causes of interference burstiness are not discussed.

Different from all this work, this article does consider the correlation of interference, uses a formal definition of burstiness, and covers different causes of interference burstiness.

## III. NETWORK MODEL

Time is divided into slots indexed by  $t \in \mathbb{Z}$ . The network consists of multiple mobile nodes communicating over a common radio channel with a certain data traffic pattern. All nodes act independently from each other. The main symbols and notations used in this article are given in Table I.

### A. Node placement and mobility

Each node has a location  $x(t) \in \mathbb{R}^2$  in slot  $t$ . The locations of all nodes form a two-dimensional Poisson point process (PPP)  $\Phi(t)$  with intensity  $\lambda$ . The use of a PPP to model node locations is motivated by the fact that most related work on interference analysis and modeling uses the Poisson process to model interference sources [34–36]. In cellular networks, the gap between PPP and more regular point processes for the base stations (interferers) is relatively small [37] and with stronger shadowing, the interference distribution in any point process approaches that of a PPP [38].

All nodes are moving in the system plane. The mean speed over all nodes and time is denoted by  $v$ . Two mobility models are used: random direction and discrete-time Brownian motion. In random direction mobility, each node moves with constant speed in a random direction sampled from a uniform distribution over all angles and keeps this direction [39; 40]. The location of a node changes from slot  $t$  to slot  $t + \Delta t$  such that  $\|x(t + \Delta t) - x(t)\| = v \Delta t$ . In Brownian motion, a node changes its location from slot  $t$  to slot  $t + 1$  [41; 42], such that  $x(t + 1) - x(t) = v \omega(t)$ , where  $\omega(t) = [\omega_1(t), \omega_2(t)]^T$  and  $\omega_1(t)$  and  $\omega_2(t)$  are i.i.d. with normal distribution  $\mathcal{N}(0, \sigma^2)$  with  $\sigma^2 = 2/\pi$ . Hence, for a given  $v$  and  $\Delta t$ , the distance between the start point  $x(t)$  and end point  $x(t + \Delta t)$  of a node is shorter on average with Brownian motion than with random direction. Both mobility models preserve the original point process: at any point in time, the node locations form a PPP with fixed intensity  $\lambda$  [41; 43; 44].

### B. Traffic

The message duration is  $d \in \mathbb{N}$  slots, which is constant for all nodes and over time. When idle, each node starts transmitting a message with probability  $u$ , independently of all other nodes. The fraction of nodes starting to transmit a message in any given slot follows as  $p = \frac{u}{1+u(d-1)}$ , and the fraction of nodes transmitting in each slot is  $\mu = pd \leq 1$ . Due to the independent transmissions, the set of transmitting nodes in each slot  $t$ , denoted by  $\Phi_{\text{TX}}(t)$ , forms a PPP of intensity  $\lambda\mu$ . This traffic model is similar to slotted random access used in many real-world systems, e.g., for initial communication to request resources, establish network associations, and re-establish failed connections to a base station [45–47]. The use of more advanced random access protocols—e.g., carrier sense multiple access—would, in general, lead to a different type of point process of the interferers. Although the interference dynamics of networks with carrier sensing has been analyzed in the literature [48], a study of the resulting burstiness is beyond of the scope of this article. Our objective is to first understand the simpler case without carrier sensing and proceed to more complex modeling assumptions in potential future work.

### C. Channel

All nodes transmit with unit power. The power attenuation over a distance follows a non-singular distance-dependent path loss model. The path loss from a transmitting node at  $x$  to the origin is  $\ell_x = \min(1, \|x\|^{-\alpha})$ , where the path loss exponent  $\alpha > 2$  is constant over all slots. The multipath propagation effects are modeled by Nakagami- $m$  fading [49]. The power received from a node located at  $x$  in slot  $t$  is  $\ell_x g_x(t)$ , where  $g_x(t)$  is the fading gain. Under Nakagami- $m$  fading, the fading gain  $g$  follows a gamma distribution ( $g \sim \Gamma(m, m)$ ) which implies  $\mathbb{E}[g] = 1$ . The parameter  $m$  determines the severeness of fading;  $m = 1$  corresponds to Rayleigh fading. For  $m \rightarrow \infty$ , we have  $g \rightarrow 1$  almost surely, which corresponds to a constant channel (no fading). From a temporal perspective, we assume a “block” fading channel, where the channel state remains constant for the duration  $c \in \mathbb{N}$  slots and then changes

to an independent value. In this sense,  $c$  represents the channel coherence time. The coherence periods are offset randomly such that a fraction  $1/c$  of the nodes change their channel state in each slot. The channel is called fast fading if  $c = 1$  and slow fading if  $c > 1$  in this article.

### D. Interference

The interference power  $I(t)$  is considered to be the aggregate of the reception powers from all transmitting nodes at time  $t$ . Without loss of generality (due to the stationarity of the PPP), we analyze the interference at the origin, which is

$$I(t) = \sum_{x \in \Phi_{\text{TX}}(t)} \ell_x g_x(t) \quad (1)$$

with our network model. The mean interference is  $\mu_I = \mu\lambda \int_{\mathbb{R}^2} \ell_x dx = \mu\lambda 2\pi \int_0^\infty \ell_r r dr = \mu\lambda \pi \frac{\alpha}{\alpha-2}$  (also see [50]). Interference power correlates over time when the node locations change slowly, the channel correlates over multiple slots, or the messages exceed one slot. The interference correlation is dictated by the parameters of the node locations (mobility model, speed  $v$ ), the wireless channel model (block length  $c$  and Nakagami  $m$  parameter), and the traffic model (message length  $d$  and fraction of transmitters  $\mu$ ) [27]. We are interested in the lag-1 auto-correlation, which we simply call correlation.

## IV. INTERFERENCE PIKES AND BURSTINESS

### A. Interference Pikes and Burstiness Claim

A continuous-valued interference power signal  $I(t)$  is discretized to a binary signal  $J(t)$  by setting a threshold  $\theta$  for the interference level that a receiver can handle. As illustrated in Fig. 1, we set  $J(t) = 1$  whenever  $I(t) > \theta$  (high interference) and  $J(t) = 0$  otherwise. In short,  $J(t) = \mathbf{1}\{I(t) > \theta\}$ . We apply thresholds that are normalized to the temporal mean  $\mu_I$  and standard deviation  $\sigma_I$  of  $I(t)$ , given as

$$\theta = \mu_I + \xi \sigma_I \quad (2)$$

with scaling parameter  $\xi \in \mathbb{R}^+$ . Following the “three sigma rule” [51], we examine different thresholds  $\theta$  with  $\xi$  up to a value of 3.

A *pike* is an interval  $\mathcal{P} = \{t_n, \dots, t_o\}$  of  $\mathbb{Z}$  with  $J(t) = 1$  for all  $t \in [t_n, t_o]$  but  $J(t_n - 1) = J(t_o + 1) = 0$ . The first slot  $t_n$  in a pike is called pike arrival. The set of all pike arrival times forms the stationary one-dimensional stochastic process  $\Phi_{\mathcal{P}}$  whose intensity is denoted by  $\lambda_{\mathcal{P}}$ . A *valley* is an interval  $\mathcal{V} = \{t_{n'}, \dots, t_{o'}\}$  of  $\mathbb{Z}$  with  $J(t) = 0$  for all  $t \in [t_{n'}, t_{o'}]$  but  $J(t_{n'} - 1) = J(t_{o'} + 1) = 1$ . This way,  $\mathbb{Z}$  is partitioned into pikes and valleys.

The pike duration  $\tau_{\mathcal{P}}$  is the cardinality of a pike, and the valley duration  $\tau_{\mathcal{V}}$  is the cardinality of a valley. The *pike interarrival time*  $\tau$  is the sum of the cardinalities of a pike and the following valley [53]. Pikes, valleys, and pike interarrival times are indexed by integers such that  $\mathcal{P}_{k+1}$  is the pike following  $\mathcal{P}_k$ ,  $\mathcal{V}_k$  is the valley following  $\mathcal{P}_k$ , and  $\tau_k$  is the sum of the cardinalities of  $\mathcal{P}_k$  and  $\mathcal{V}_k$ . Symbols without indices refer to the typical instances of the random variables.

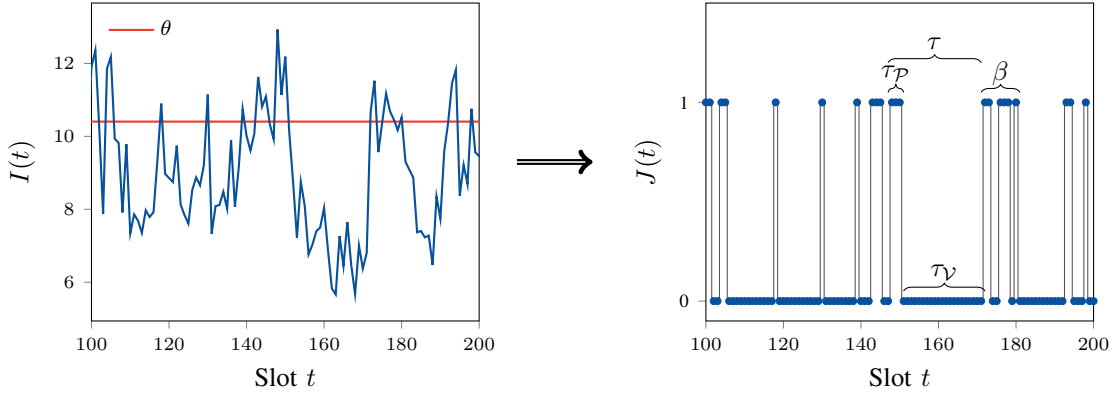


Fig. 1: A continuous-valued interference power signal  $I(t)$  is transformed into a binary signal  $J(t)$  using the threshold  $\theta$ . Conceptual illustration of pike duration  $\tau_P$ , valley duration  $\tau_V$ , pike interarrival time  $\tau$ , and burst size  $\beta$  ( $\delta = 4$ ).

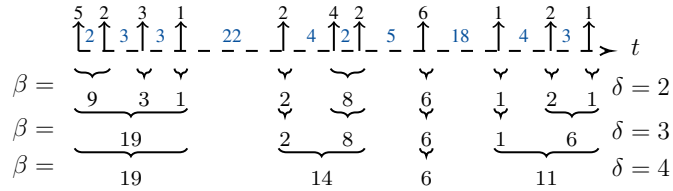


Fig. 2: Burst size  $\beta$  for different valley duration threshold  $\delta$ . Here the arrows indicate the pike arrivals, with pike durations  $\tau_{P_k}$  on top of it. The valley durations  $\tau_{V_k}$  are shown in between the arrows. Inspired by [52].

Our preparatory work [14] claims that “interference pikes arrive in bursts” for the network model in that paper. In simple terms, it is likely that there occur several pikes in a short time followed by a long valley. This behavior is of particular interest in interference-limited wireless networks, and to understand it, we should *quantify and analyze* the degree of burstiness of pike arrivals in order to find the origin of this phenomenon. This could contribute toward a better understanding of interference dynamics and in turn improve the design of reliability techniques.

### B. How to Quantify Burstiness?

The bursty nature of events has been analyzed in various disciplines using different measures and methods. One branch of science that intends to understand the roots of bursty patterns is the theory of temporal networks [54; 55]. Here, many empirical event sequences are non-Poisson or bursty [5; 53; 55]. Examples include activity patterns of single neuron firings [4], solar flares [3], earthquakes [1; 2], and email communications [6]. The arrival of events in these systems can be characterized by the probability distribution and the correlation of the interarrival times  $\tau$  [28]. The distribution shows the likelihood of particular  $\tau$ -values, and the correlation informs about their temporal order, e.g., whether short  $\tau$ -values tend to be followed by short ones. In this way, the characteristics of the distribution and the correlation can individually or jointly be a reason for bursty (or non-bursty) event sequences. The deviation of the distribution from the

exponential distribution resulting from a Poisson process can be characterized by a burstiness measure; and the correlation coefficient is sometimes called memory coefficient or simply memory [28]. We are interested in these two measures along with a third, the burst size, as defined in the following.

A *burstiness measure* based on the mean  $\bar{\tau}$  and standard deviation  $\sigma_\tau$  of the interarrival time can be defined as [28]

$$B = \frac{\frac{\sigma_\tau}{\bar{\tau}} - 1}{\frac{\sigma_\tau}{\bar{\tau}} + 1} = \frac{\sigma_\tau - \bar{\tau}}{\sigma_\tau + \bar{\tau}} \quad (3)$$

with value range  $B \in [-1, 1]$ . This measure is a normalized form of the coefficient of variation  $\sigma_\tau/\bar{\tau}$  used in statistics. The value  $B = 1$  corresponds to the highest burstiness, whereas  $B = -1$  is obtained for completely regular (periodic) arrivals. For Poisson arrivals,  $B = 0$  since  $\bar{\tau} = \sigma_\tau$  for the exponential distribution. For a finite number of arrivals  $\nu$ , an estimator of  $B$  is [29]

$$\hat{B} = \frac{\sqrt{\nu+1} \frac{\hat{\sigma}_\tau}{\hat{\tau}} - \sqrt{\nu-1}}{(\sqrt{\nu+1} - 2) \frac{\hat{\sigma}_\tau}{\hat{\tau}} + \sqrt{\nu-1}} \quad (4)$$

provided that  $\nu > \sigma_\tau^2/\bar{\tau}^2$ , where  $\hat{\tau}$  and  $\hat{\sigma}_\tau$  are estimates of  $\bar{\tau}$  and  $\sigma_\tau$ , respectively.

The *memory coefficient*  $M$  is defined as the Pearson correlation coefficient between two consecutive  $\tau$ :

$$M = \frac{\mathbb{E}[(\tau_j - \bar{\tau})(\tau_{j+1} - \bar{\tau})]}{\sigma_\tau^2}, \quad (5)$$

which takes a value in the range  $[-1, 1]$ . A positive value of  $M$  means short  $\tau$  tend to follow short  $\tau$  and vice versa, resulting in a bursty behavior. A negative value of  $M$  means short (long)  $\tau$  tend to follow long (short)  $\tau$ , resulting in a more regular behavior. Poisson arrivals would lead to  $M = 0$ . In case of a finite number of arrivals  $\nu$ , we adopt the commonly used estimator  $\hat{M} = \frac{1}{\nu-1} \sum_{j=1}^{\nu-1} (\tau_j - \hat{\tau})(\tau_{j+1} - \hat{\tau})/\hat{\sigma}_\tau^2$ .

A sequence of consecutive pikes separated from each other with valley durations smaller than or equal to some threshold  $\delta > 1$  is called *burst* or pike train [53; 56]. The *burst size*  $\beta$  is the number of slots from the beginning of the first pike until the end of the last pike in a burst, where each burst ends right before a valley that is longer than  $\delta$ , as illustrated in Fig. 2. Let  $\mathcal{L} = \{i \in \mathbb{Z}: \tau_{V_i} > \delta\}$  be the indices of the valleys

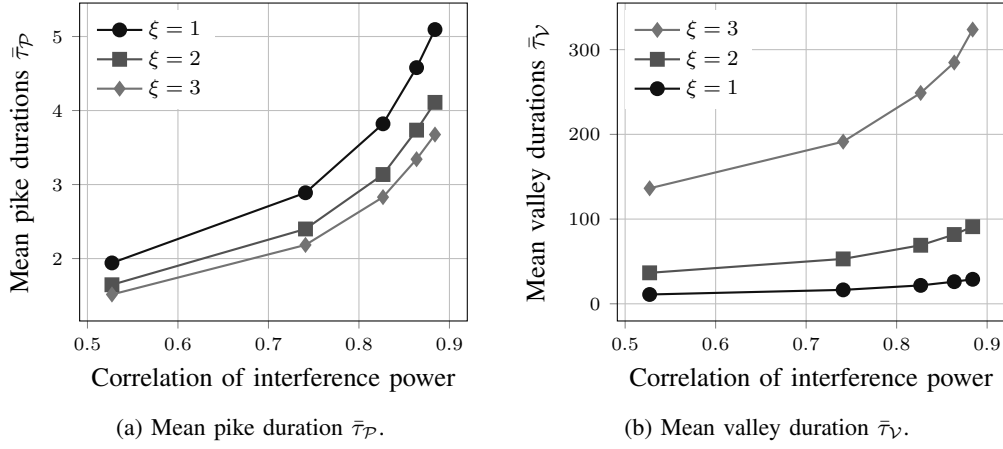


Fig. 3: Mean pike and valley duration versus correlation for basic network scenario. Here,  $\lambda = 1$ ,  $\alpha = 3$ ,  $v = 0$ ,  $m = 1$ ,  $c = 15$ ,  $\mu = 0.5$  and  $d \in \{2, 5, 9, 13, 17\}$ .

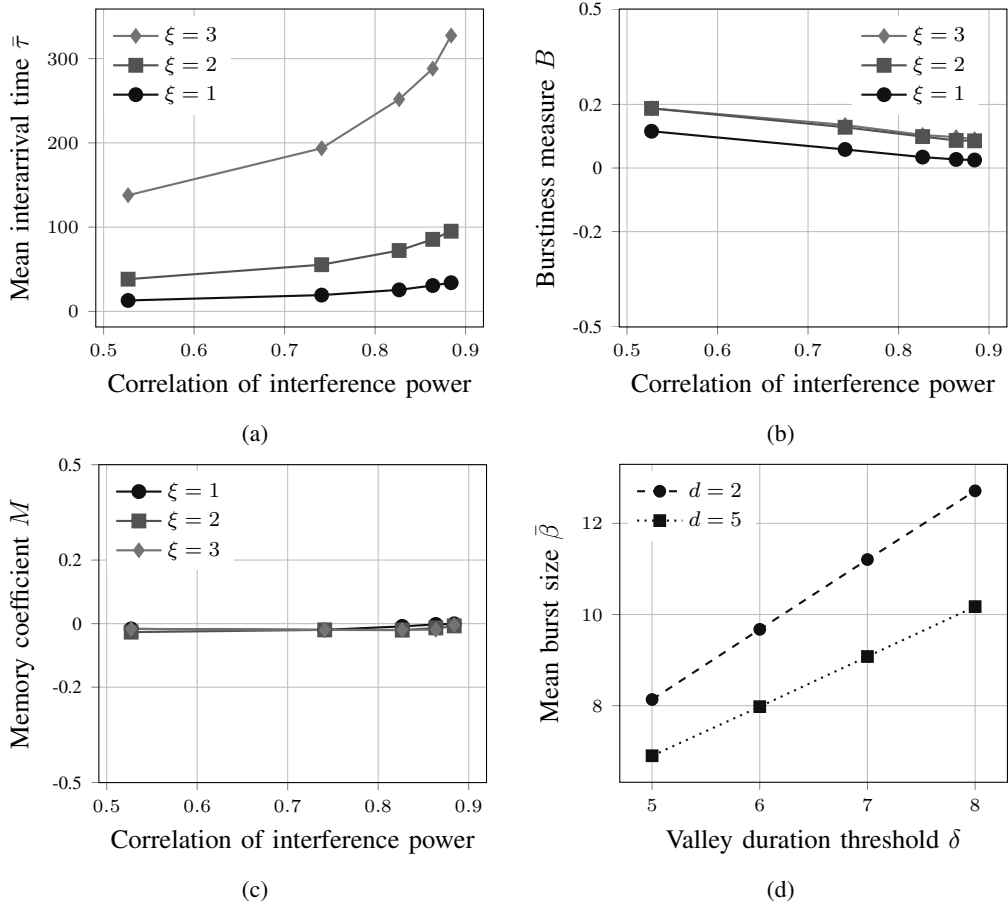


Fig. 4: Mean interarrival time  $\bar{\tau}$ , burstiness measure  $B$ , memory coefficient  $M$  and mean burst size  $\bar{\beta}$  for the basic network scenario. Here,  $\lambda = 1$ ,  $\alpha = 3$ ,  $v = 0$ ,  $m = 1$ ,  $c = 15$ ,  $\mu = 0.5$  and  $d \in \{2, 5, 9, 13, 17\}$ .

longer than  $\delta$ . Assume  $\mathcal{L}$  is ordered and denote its elements by  $\{b_k\}_{k \in \mathbb{Z}}$ . Then  $\mathcal{B}_k = (\mathcal{P}_{b_k+1}, \mathcal{P}_{b_k+2}, \dots, \mathcal{P}_{b_{k+1}})$  is the  $k$ -th burst, and its length is  $\beta_k = \max\{\mathcal{P}_{b_{k+1}}\} - \max\{\mathcal{V}_{b_k}\}$ .

In summary, we consider two conceptually distinct reasons for bursty arrivals: certain non-exponential distributions of  $\tau$  leading to high  $B$  and positive correlation of  $\tau$  corresponding to high  $M$ . As a third measure, the burst size is used to further

characterize the temporal dynamics. We apply all three measures in our analysis of wireless interference and the search for the causes of its apparent burstiness. The computational complexity to evaluate these metrics is  $O(N)$ , where  $N$  is the number of slots.

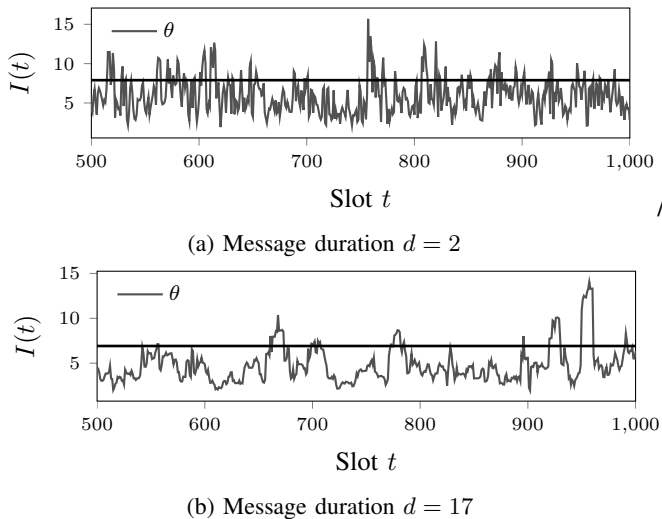


Fig. 5: Interference power for basic network scenario.

## V. MODEL-BASED ANALYSIS OF INTERFERENCE BURSTS

### A. Simulation Setup

Our simulation takes place in the square  $[-a, a]^2$  of area  $A = 4a^2$  with wrap-around borders. If a mobile node reaches one side of the square, it continues moving and reappears on the opposite side to avoid boundary effects [39; 57]. The number of nodes is chosen from a Poisson distribution with parameter  $\lambda A$ . We use a node intensity  $\lambda = 1$  and choose a path loss exponent  $\alpha = 3$  suited for many environments. Furthermore, we demand the area to be large enough to result in an expected interference that is only slightly lower than the one caused by nodes on an infinite plane. Specifically, we request:  $\int_{[-a, a]^2} \ell_x dx > 0.98 \int_{\mathbb{R}^2} \ell_x dx$ . The fraction of the mean interference by Poisson interferers located outside the square is  $\frac{4\sqrt{2}}{3\pi a} \approx \frac{0.6}{a}$ , which yields 1.2% for a square with  $a = 50$ , which we choose. In the following we estimate the properties of interference pike arrivals in different scenarios. For simplicity of mathematical notation, the hat on the corresponding symbols is omitted. All results are averaged over 100,000 slots and 100 realizations of  $\Phi$ .

### B. Analysis for a Basic Static Network

In a first simulation, all nodes are static and both channel and traffic are correlated over multiple slots ( $c > 1$  and  $d > 1$ ). Figs. 3–5 show the properties of interference pikes. The results can be summarized as follows.

Once the interference power crosses the threshold  $\theta$ , the higher the correlation, the longer it will stay on this side of  $\theta$  on average. Hence, all durations  $\bar{\tau}_P$ ,  $\bar{\tau}_V$ , and  $\bar{\tau}$  increase with increasing correlation irrespective of  $\xi$  (see Figs. 3a, 3b, and 4a). The higher  $\xi$ , the fewer pikes occur, and, if one does occur, the interference stays above  $\theta$  for a short time only, which results in shorter pikes (Fig. 3a) and longer valleys (Fig. 3b), which here leads to longer  $\tau$  (Fig. 4a).

The burstiness  $B$  decreases with increasing interference correlation (Fig. 4b). From left to right, the traffic alters from fast varying ( $d = 2$ ) to slowly varying ( $d = 17$ ), while the

channel always varies slowly ( $c = 15$ ). For short messages, the interference dynamics is a combination of slow fading and fast traffic variations (Fig. 5a). It is this overlay of slow and fast variations that causes the clustering of pikes. In contrast, for long messages, both channel and traffic vary slowly (Fig. 5b), resulting in a lower burstiness with high interference correlation. The burstiness increases with increasing  $\xi$  (Fig. 4b) because a high threshold separates clustered pikes by long valleys, which represents a bursty behavior.

The memory coefficient  $M$  remains flat at  $M \approx 0$  (Fig. 4c). This means that the bursty appearance of pikes is contributed entirely to the distribution of  $\tau$ .

The mean burst size  $\bar{\beta}$  (Fig. 4d for  $\xi = 1$ ) is bigger for short messages ( $d = 2$ ) than for longer ones ( $d = 5$ ). Interestingly, this means that outages can be longer for short messages although individual pikes are typically shorter. Recall that bursts become longer with increasing  $\delta$  since more pikes become part of a single burst. Bursts become shorter with increasing  $\xi$  given the fact that pikes become longer and valleys shorter.

### C. Interim Discussion and Next Steps

This first analysis gave some insights into the burstiness of interference pikes. However, several issues remain unclear: Does  $B$  always decrease with the correlation? Does  $B$  depend on the source of correlation? Is the burstiness of pike arrivals only attributed to the distribution of  $\tau$ ? Is there any memory  $M$  in the sequence of  $\tau_k$ -values?

To address these issues, we analyze different network scenarios shown in Table II. In principle, each component of the network model—node locations, channel, and traffic—can be classified according to its temporal dynamics: the values can be constant, slowly varying, or fast varying over time. For example, nodes at constant random locations ( $v = 0$ ) send over a slow fading channel ( $m$  finite,  $c > 1$ ) with constant traffic ( $\mu = 1$ ). Or, mobile nodes ( $v > 0$ ) send over a fast fading channel ( $m$  finite,  $c = 1$ ) with fast varying traffic ( $\mu < 1$ ,  $d = 1$ ). All cases considered are based on stochastic models except for two extremes that are deterministic:  $m \rightarrow \infty$  (constant channel) and  $\mu = 1$  (constant traffic). Deterministic models leading to non-constant values are not considered.

The fundamental question is which models and parameters contribute to the interference correlation. In general: Stochastic models with parameters leading to fast variations do not contribute to the correlation of the interference power, since a random value is chosen in each slot independent of the previous slot in our network model, which implies no correlation between two slots. Models with parameters leading to slow variations (slower than a slot length) are sources of interference correlation.

We proceed as follows: First, we analyze a single source of correlation (locations in Scenario  $\mathcal{S}1$ , channel in  $\mathcal{S}2$ , and traffic in  $\mathcal{S}3$ ). Second, we consider a combination of multiple sources of correlation (channel and traffic in Scenario  $\mathcal{M}1$  and all three sources in  $\mathcal{M}2$ ). Additionally, we also analyzed different values of path loss exponent  $\alpha$  and node density  $\lambda$ . We find that these parameters do not have much effect on the

TABLE II: Overview of analyzed network scenarios. Parameters: Mean node speed  $v$ , Nakagami- $m$  parameter, channel block length  $c$  in slots, fraction of transmitting nodes  $\mu$ , and message duration  $d$  in slots. Parameters marked with a dash are irrelevant (an arbitrary positive integer value can be chosen).

Scenario	Case description	Node $v$	Model parameters				Case index [27]		
			Channel $m$	$c$	Traffic $\mu$	$d$	Node $i$	Channel $j$	Traffic $k$
$\mathcal{S}_1$	Mobile nodes send over a constant channel with constant traffic	$> 0$	$\infty$	–	1	–	2	0	0
	Mobile nodes send over a fast Rayleigh channel with constant traffic	$> 0$	1	1	1	–		1	0
	Mobile nodes send over a constant channel with fast varying traffic	$> 0$	$\infty$	–	$< 1$	1		0	1
$\mathcal{S}_2$	Static nodes send over a slow Rayleigh channel with constant traffic	0	1	$> 1$	1	–	0	2	0
	Static nodes send over a slow Rayleigh channel with fast varying traffic	0	1	$> 1$	$< 1$	1			0
$\mathcal{S}_3$	Static nodes send over a constant channel with slowly varying traffic	0	$\infty$	–	$< 1$	$> 1$	0	0	2
	Static nodes send over a fast Rayleigh channel with slowly varying traffic	0	1	1	$< 1$	$> 1$			
$\mathcal{M}_1$	Static nodes send over a slow Rayleigh channel with slowly varying traffic	0	1	$> 1$	$< 1$	$> 1$	0	2	2
$\mathcal{M}_2$	Mobile nodes send over a slow Rayleigh channel with slowly varying traffic	$> 0$	1	$> 1$	$< 1$	$> 1$	2	2	2

correlation (which is also shown in [27]) and burstiness of interference pikes. The plots are not shown, since they do not add value to the manuscript. We use a threshold scaling of  $\xi = 1$  unless stated otherwise.

In order to establish a cross-link to our previous publications in interference dynamics [27; 58], each case in Table II is indexed by the triplet  $(i, j, k)$ , where  $i$  represents the node locations,  $j$  is the channel, and  $k$  is the traffic. We use  $i, j, k \in \{0, 1, 2\}$  with the following meaning [27]:

- 0  $\rightarrow$  Values remain constant.
- 1  $\rightarrow$  Values are randomly changing but uncorrelated.
- 2  $\rightarrow$  Values are randomly changing and correlated.

A value of 0 (constant) for the node locations means they are initially chosen from a random distribution but then remain fixed over time ( $v = 0$ ), whereas for channel and traffic, it refers to the deterministic cases of no fading and all nodes always transmitting, respectively.

#### D. Analysis for a Single Source of Correlation

An analysis of the scenarios with a single source of correlation (either  $i, j$  or  $k = 2$ ) helps us understand the effects of the different sources on interference pikes. The other two models lead to constant or fast changing values (states 0 and 1), to depict the different effects of these two options.

##### 1) Node locations as the sole correlation source

In Scenario  $\mathcal{S}_1$ , the nodes follow either of the mobility models. Channel and traffic are either constant or fast varying at random. This scenario accounts for three cases in  $(2, \{0, 1\}, \{0, 1\})$  except  $(2, 1, 1)$ . The interference is fully correlated for static nodes ( $v = 0$ ), and the correlation decreases with increasing speed. The analysis of interference pikes is shown in Fig. 6.

The mean interarrival time  $\bar{\tau}$  increases with increasing correlation in all six setups (Fig. 6a). The behavior of the burstiness  $B$  depends on the particular setup (Fig. 6b). In case  $(2, 1, 0)$ ,  $B$  increases with increasing correlation. In the

other two cases  $(2, 0, \{0, 1\})$ ,  $B$  is almost independent of the correlation within the considered range. Pikes tend to arrive in bursts for case  $(2, 1, 0)$  with Brownian motion and high correlation (low  $v$ ). Here the slow variations in node locations overlay with the fast channel variations. In this case, the pike arrivals for the two mobility models are illustrated in Fig. 7. All other setups lead to non-bursty pike arrivals. In case  $(2, 0, 0)$ , no fast variation of any model is involved. In case  $(2, 0, 1)$ , we conjecture that the effect of the faster varying traffic is compensated by the higher speed.

In all three cases, Brownian motion leads to a positive memory coefficient  $M > 0$  (Fig. 6c), which means short (long) pikes are followed by short (long) ones. In contrast, random direction mobility always has  $M \approx 0$ . The mean burst size  $\beta$  for case  $(2, 1, 0)$  with Brownian motion depends on  $v$  and  $\delta$  (Fig. 6d). Bursts tend to be longer for slow nodes since slowly changing locations cause more pikes to cluster.

##### 2) Channel as the sole correlation source

In Scenario  $\mathcal{S}_2$ , the channel remains constant for multiple slots and then randomly changes to an independent value, independently for each node (slow fading). All nodes are static and traffic is constant or fast varying. This scenario includes the two cases  $(0, 2, \{0, 1\})$ . Results are shown in Fig. 8 (green curves).

Again, the mean interarrival time  $\bar{\tau}$  increases with increasing interference correlation in both cases (Fig. 8a). The burstiness  $B$  also increases with interference correlation but its specific behavior depends on the traffic model (Fig. 8b). With constant traffic ( $k = 0$ ), the variation of the interference power is caused by the channel only (Fig. 9a). The longer the channel block size  $c$ , the more slowly the channel fades and therefore the higher the interference correlation, essentially resulting in non-bursty pikes. With fast varying traffic ( $k = 1$ ), the set of active nodes changes in every slot, resulting in a rapid variation of the interference power (Fig. 9b). It is the combination of these rapid changes in traffic with slow fading (for large  $c$ )

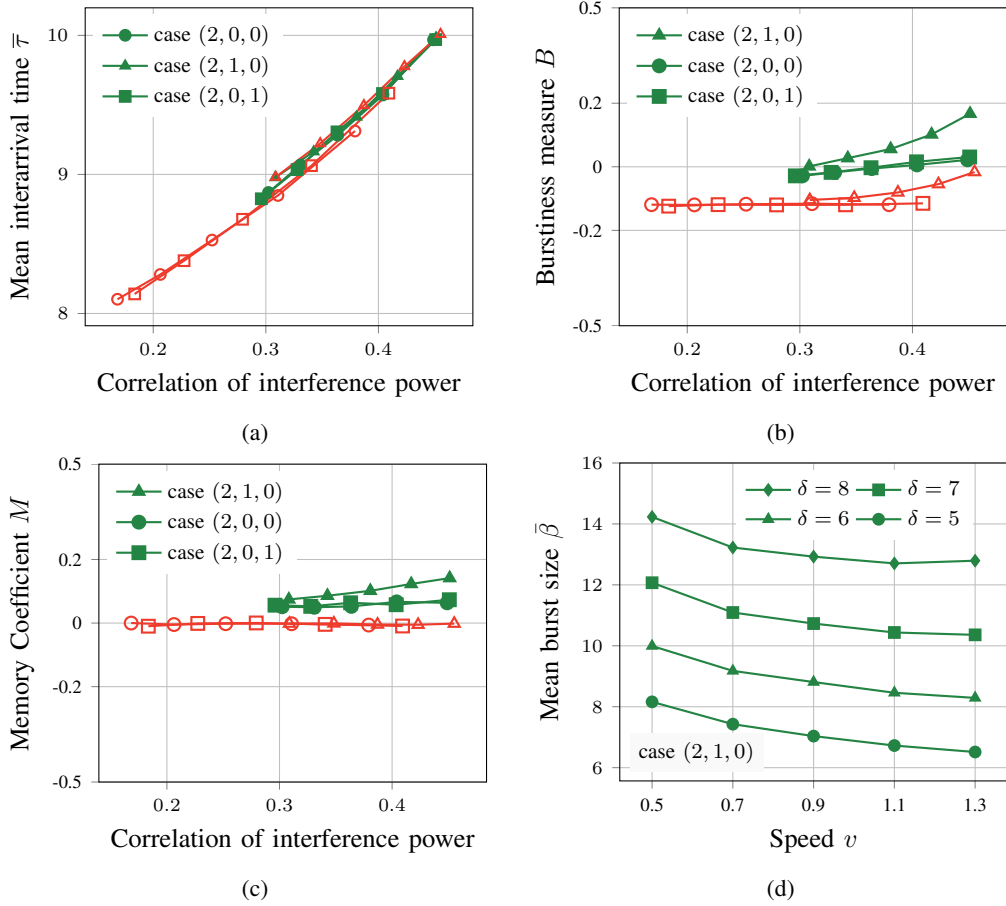


Fig. 6: Mean interarrival time  $\bar{\tau}$ , burstiness measure  $B$ , memory coefficient  $M$  and mean burst size  $\bar{\beta}$  for the three cases in Scenario  $\mathcal{S}1$  with random direction mobility (red) and Brownian motion (green). Here  $\lambda = 1$ ,  $\alpha = 3$  and  $\xi = 1$ . For case (2, 0, 0),  $m = \infty$ ,  $\mu = 1$  and  $v \in \{1.9, 2.1, 2.3, 2.5, 2.7\}$ . For case (2, 1, 0),  $m = 1$ ,  $c = 1$ ,  $\mu = 1$  and  $v \in \{0.5, 0.7, 0.9, 1.1, 1.3\}$ . For case (2, 0, 1),  $m = \infty$ ,  $\mu = 0.9$ ,  $d = 1$  and  $v \in \{1.7, 1.9, 2.1, 2.3, 2.5\}$ .

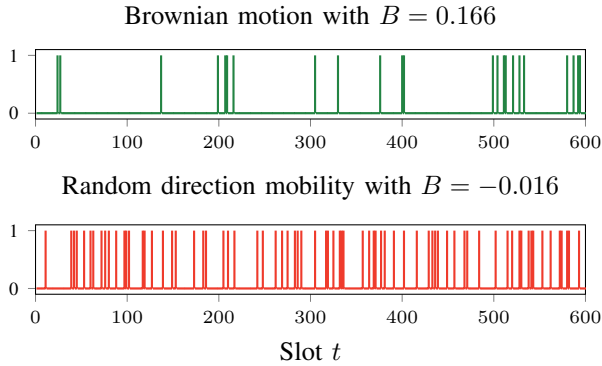


Fig. 7: Pike arrivals for Brownian motion (green) and random direction mobility (red) for case (2, 1, 0) in scenario  $\mathcal{S}1$ .

that leads to clustering of pikes ( $B > 0$ ).

The memory  $M$  in these cases is around zero or even negative for fast varying traffic (Fig. 8c). Negative  $M$  means that a short (long)  $\tau$  is typically followed by a long (short)  $\tau$ .

The bursts for fast varying traffic for a given  $\delta$  tend to get longer for increasing  $c$  (Fig. 8d). For increasing  $c$ , the pike and valley durations tend to increase, which in turn leads to

an increased  $\bar{\beta}$ . If we increase the parameter  $\delta$ , more pikes are grouped in a single burst, hence  $\bar{\beta}$  increases by definition.

### 3) Traffic as the sole correlation source

In Scenario  $\mathcal{S}3$ , the traffic is slowly changing at random with message length  $d > 1$  and constant  $\mu = 0.1$ . All nodes are static and the channel is either constant or fast fading. This scenario accounts for the two cases (0,  $\{0, 1\}$ , 2). A constant  $\mu$  results in constant mean interference, but its correlation increases with increasing  $d$ . Results are shown in Fig. 8 (orange curves).

As in the previous scenarios, the mean interarrival time  $\bar{\tau}$  increases with increasing correlation in both cases (Fig. 8a). The burstiness  $B$  depends on the channel model (Fig. 8b). A non-fading channel ( $j = 0$ ) leads to non-bursty pikes. In this case, traffic is the sole source of variation in the interference power. With increasing  $d$  but constant  $\mu = 0.1$ , the set of active nodes changes slowly, resulting in slow variations of the interference power (Fig. 10a). A fast fading channel ( $j = 1$ ) can lead to bursty pikes. In this case, the quickly varying channel combined with slowly changing traffic results in a clustering of pikes (Fig. 10b).

The memory  $M$  and mean burst size  $\bar{\beta}$  show a similar behavior as in the previous scenario (Figs. 8c and 8d). The

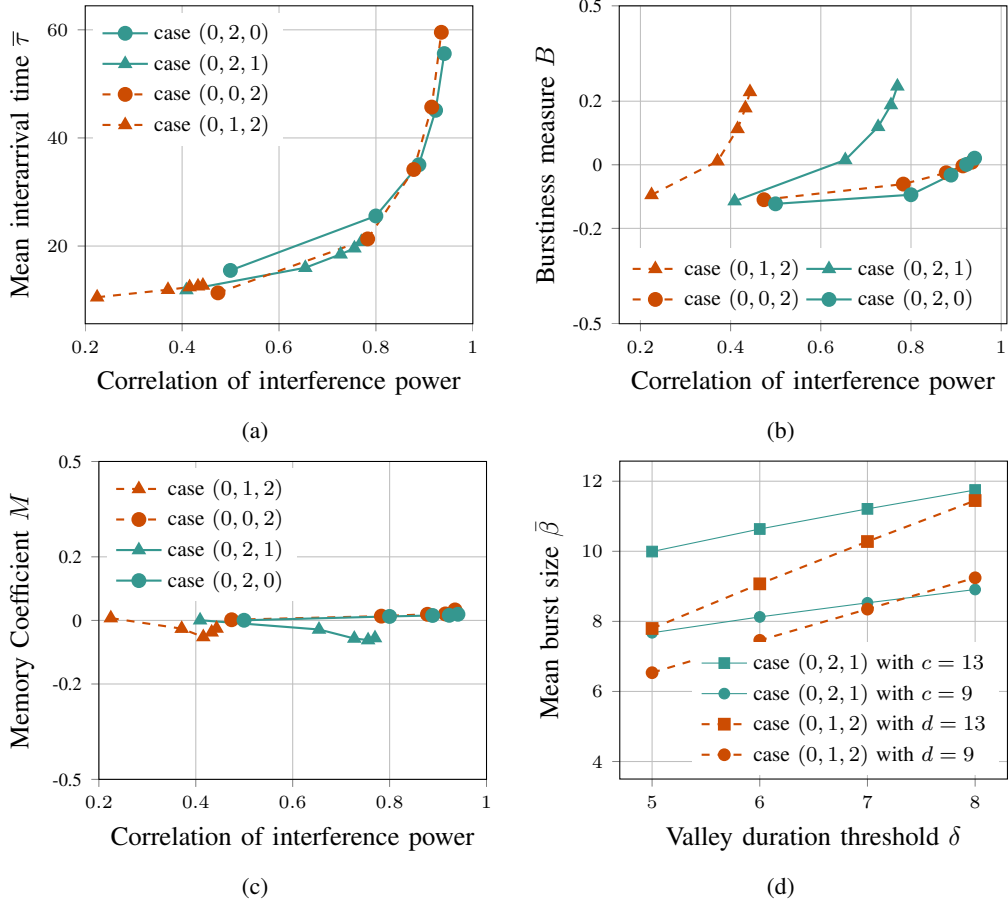


Fig. 8: Mean interarrival time  $\bar{\tau}$ , burstiness measure  $B$ , memory coefficient  $M$  and mean burst size  $\bar{\beta}$  for Scenarios  $\mathcal{S}2$  (green) and  $\mathcal{S}3$  (orange). Here,  $\lambda = 1$ ,  $v = 0$ ,  $\alpha = 3$  and  $\xi = 1$ . For case (0, 2, 0):  $m = 1$ ,  $c \in \{2, 5, 9, 13, 17\}$  and  $\mu = 1$ . For case (0, 2, 1)  $m = 1$ ,  $c \in \{2, 5, 9, 13, 17\}$ ,  $\mu = 0.9$  and  $d = 1$ . For case (0, 0, 2):  $m = \infty$ ,  $\mu = 0.1$  and  $d \in \{2, 5, 9, 13, 17\}$ . For case (0, 1, 2):  $m = 1$ ,  $c = 1$ ,  $\mu = 0.1$  and  $d \in \{2, 5, 9, 13, 17\}$ .

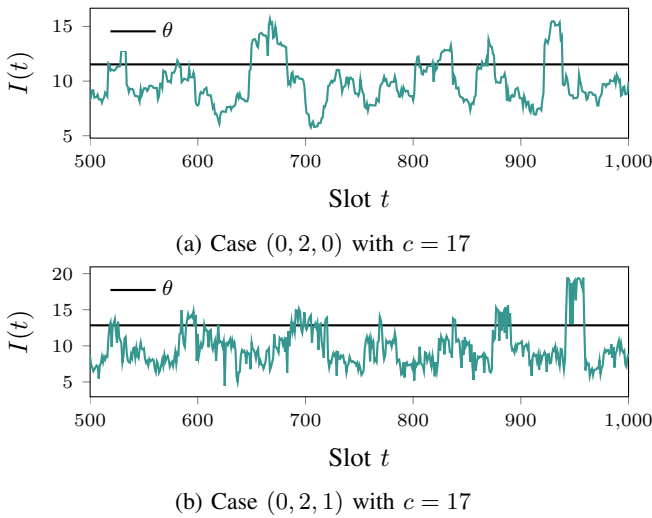


Fig. 9: Interference power for Scenario  $\mathcal{S}2$  with  $\xi = 1$ .

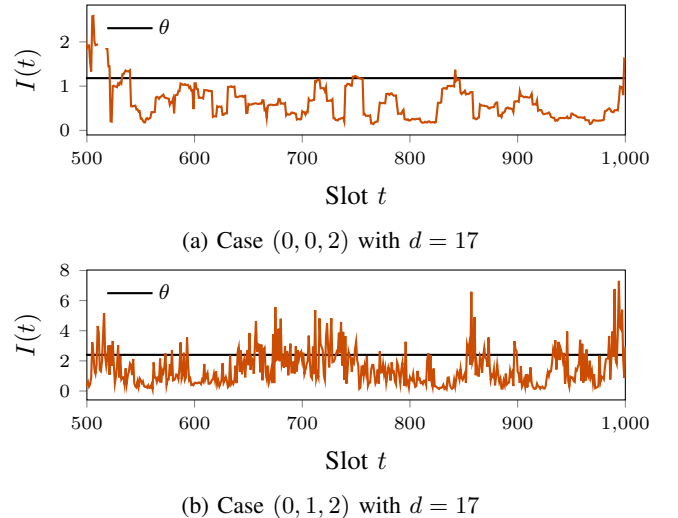


Fig. 10: Interference power for Scenario  $\mathcal{S}3$  with  $\xi = 1$ .

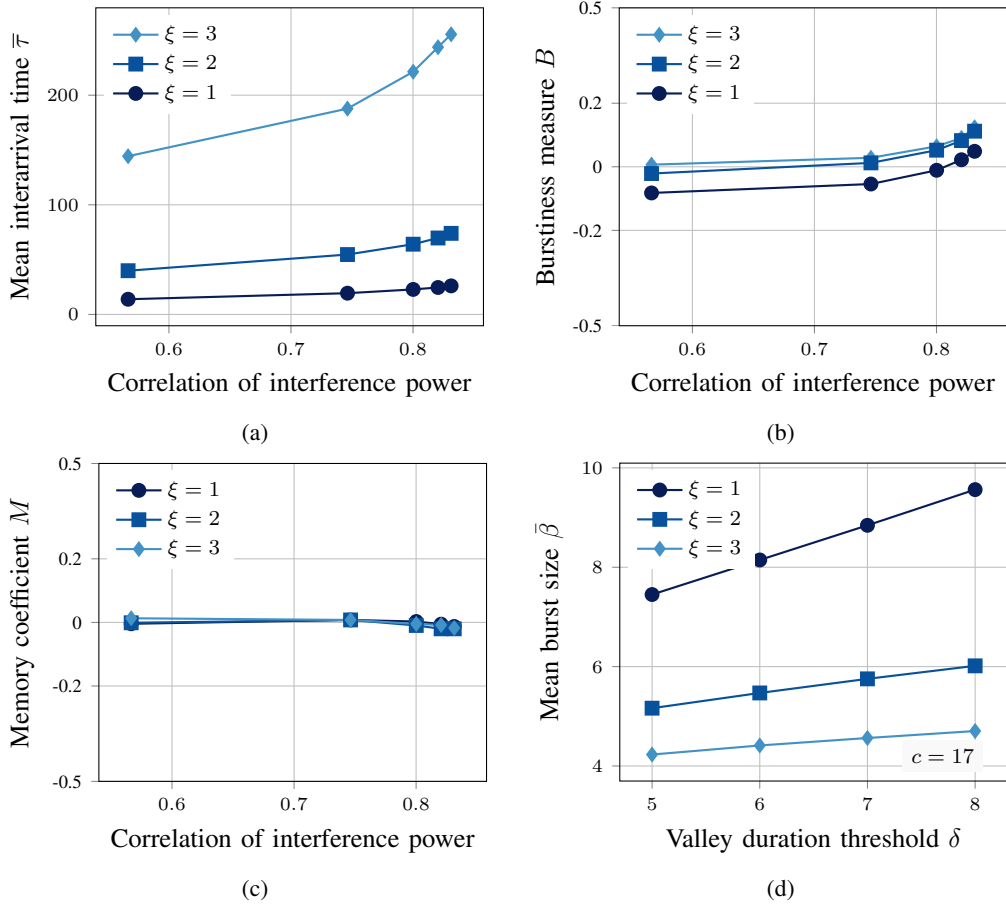


Fig. 11: Mean interarrival time  $\bar{\tau}$ , burstiness measure  $B$ , memory coefficient  $M$  and mean burst size  $\bar{\beta}$  for case  $(0, 2, 2)$  in Scenario  $\mathcal{M}1$ . Here  $\lambda = 1$ ,  $\alpha = 3$ ,  $v = 0$ ,  $\mu = 0.5$ ,  $d = 9$ ,  $m = 1$  and  $c \in \{2, 5, 9, 13, 17\}$ .

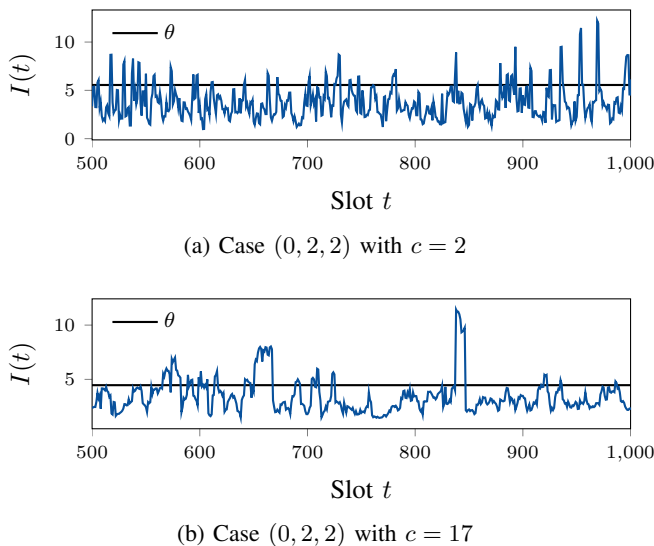


Fig. 12: Interference power for  $\mathcal{M}1$  with  $\xi = 1$ .

bursts tend to get longer for longer messages.

Comparing Scenario  $\mathcal{S}2$  with Scenario  $\mathcal{S}3$  in Fig. 8b, it can be observed that  $B$  is similar for both cases  $(0, 1, 2)$  and  $(0, 2, 1)$  irrespective of the source of correlation. Pikes arrive in bursts for low correlation for case  $(0, 1, 2)$  as compared to

case  $(0, 2, 1)$ .

### E. Analysis for Multiple Sources of Correlation

#### 1) Channel and traffic as correlation sources

In Scenario  $\mathcal{M}1$ , both channel and traffic change slowly (with  $c > 1$  and  $d > 1$ ); they thus both contribute to the correlation. The nodes are static. This accounts for case  $(0, 2, 2)$ .

As always, the mean interarrival time  $\bar{\tau}$  increases with increasing correlation (Fig. 11a). The burstiness  $B$  also increases with increasing correlation (Fig. 11b). Two setups can be distinguished: If the channel is expected to change faster than the traffic ( $c < d$ ), the interference crosses the threshold frequently (Fig. 12a), and we obtain regular arrivals of pikes ( $B < 0$ ). If the channel changes more slowly than the traffic ( $c > d$ ), the interference also changes more slowly (Fig. 12b), and we obtain bursty arrivals of pikes ( $B > 0$ ).

The memory  $M$  is about zero over the considered range of  $c$  (Fig. 11c). Fig. 11d shows the mean burst size  $\bar{\beta}$  with  $c = 17$  for different  $\delta$ .  $\bar{\beta}$  is the lowest for  $\xi = 3$  because the interference power seldom crosses the threshold (long valleys) and also for short duration of time (short pikes).

#### 2) Locations, channel, and traffic as correlation source

In Scenario  $\mathcal{M}2$ , all three models contribute towards correlation, which accounts for case  $(2, 2, 2)$ . The channel and

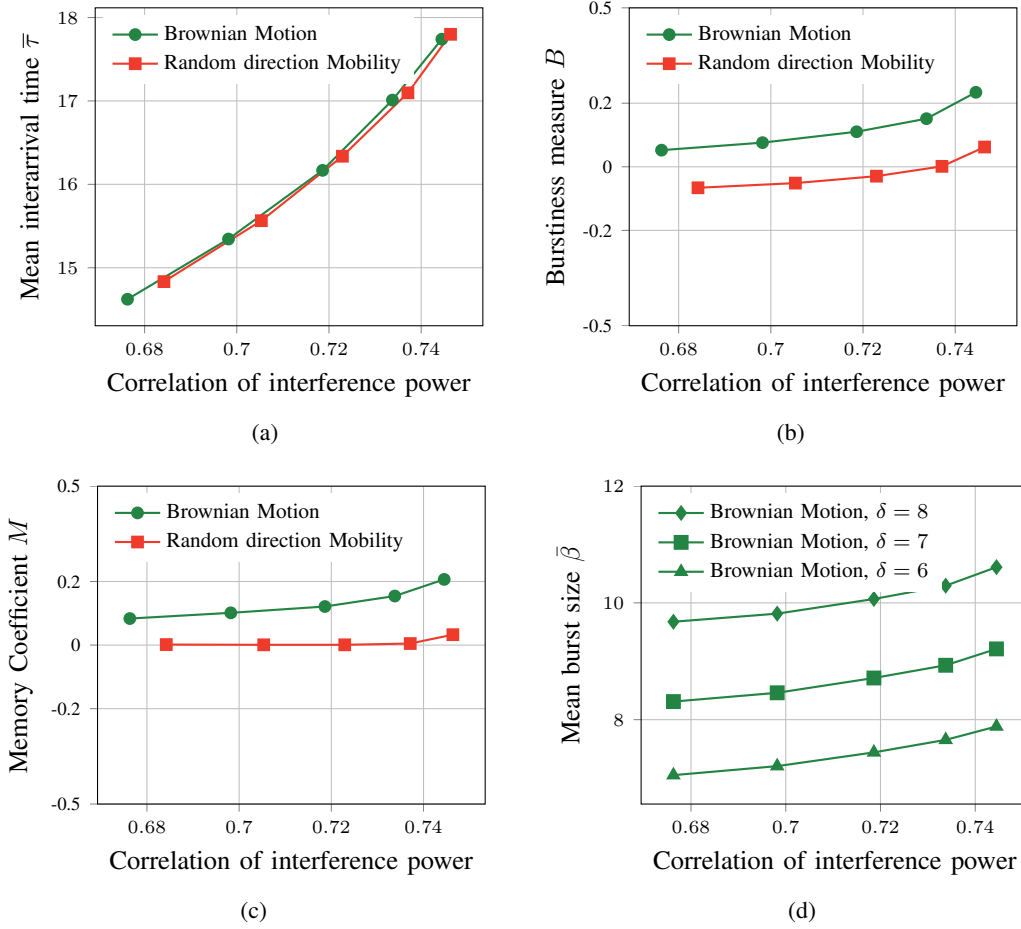


Fig. 13: Mean interarrival time  $\bar{\tau}$ , burstiness measure  $B$ , memory coefficient  $M$  and mean burst size  $\bar{\beta}$  for case  $(2, 2, 2)$  in Scenario  $\mathcal{M}2$  with random direction mobility (red) and Brownian motion (green). Here  $\lambda = 1$ ,  $\alpha = 3$ ,  $\xi = 1$ ,  $v \in \{0.1, 0.2, 0.3, 0.4, 0.5\}$ ,  $\mu = 0.5$ ,  $d = 5$ ,  $m = 1$  and  $c = 5$ .

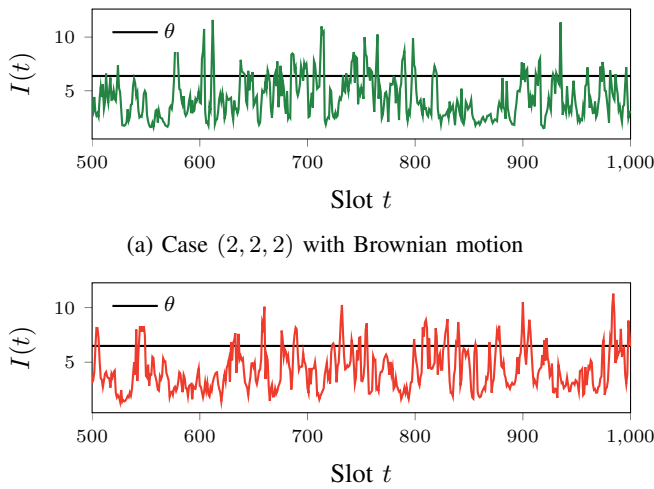


Fig. 14: Interference power for Scenario  $\mathcal{M}2$ .

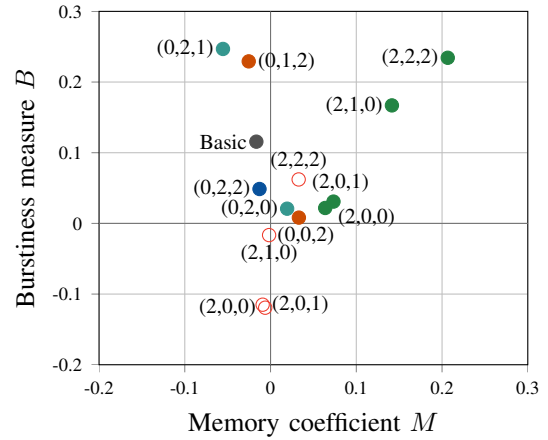


Fig. 15: Burstiness measure  $B$  versus memory coefficient  $M$  for the network scenarios given in Table II. For mobile interferers ( $i = 2$ ), empty marks represent random direction mobility and solid marks represent Brownian motion. 'Basic' indicates the analysis of the basic static network in Section V-B.

traffic vary slowly with  $c > 1$  and  $d > 1$ . The nodes follow either of the two mobility models with their correlation considered.

As in the previous scenario, the mean interarrival time  $\bar{\tau}$  (Fig. 13a) and burstiness  $B$  (Fig. 13b) increase with increasing correlation for both setups. Pikes arrive in bursts for Brownian motion and in a regular fashion for random direction mobility (except for very low speed  $v = 0.1$ ). Traces of the interference power for both models are shown in Fig. 14.

The memory  $M$  is positive for Brownian motion (Fig. 13c), indicating that burstiness of pikes is contributed by both the distribution of  $\tau$  and memory in  $\tau_k$ . It is zero for random direction mobility except for very low speed ( $v = 0.1$ ). Bursts tend to be longer at low speed (high correlation) for Brownian motion (Fig. 13d).

### F. Summary of Burstiness and Memory

Fig. 15 shows for each setup the highest observed  $B$  and the corresponding  $M$ . Some observations can be made: First, static interferers ( $i = 0$ ) result in high burstiness of pikes when the channel or traffic have fast variations. Second, mobile interferers ( $i = 2$ ) with Brownian motion result in higher burstiness of pikes compared to random direction mobility and always result in positive  $M$ .

Table III presents a summary of the effect of correlation  $\rho$  on  $B$  for all the scenarios analyzed above. Overall it is observed that  $B$  increases with increasing correlation  $\rho$ , except for the basic scenario. Here,  $\rho$  increases with increasing  $d$  but at the same time the traffic changes slowly. Hence, with increasing  $d$ , slow varying traffic overlaps with a slowly varying channel ( $c = 15$ ), resulting in decreasing  $B$  with increasing  $\rho$ .

## VI. EXPERIMENTAL ANALYSIS OF INTERFERENCE BURSTS

### A. Setup

Finally, we analyze the arrival of interference pikes in a mobile phone connected to a commercial 4G cellular network. This analysis helps us to identify whether the burstiness is rooted in the modeling assumptions or measured interference shows similar behavior.

We analyze the interference pikes for an automotive driving in two European countries, Austria and Albania. Measurements were conducted in two different automotive environments: freeway and urban area. In the freeway scenario  $\mathcal{F}$ , we drove on the Austrian Südbahn A2 between Wolfsberg and Klagenfurt with an average speed of 93 km/h denoted  $\mathcal{F}_1$  (Fig. 16a), and on the Albanian freeway between Tirana and Fier with an average speed of 77 km/h denoted  $\mathcal{F}_2$  (Fig. 16c). In the urban scenario  $\mathcal{U}$ , we drove in the city of Klagenfurt with an average speed of 27 km/h denoted  $\mathcal{U}_1$  (Fig. 17a), in the city of Linz with an average speed of 9 km/h denoted  $\mathcal{U}_2$  (Fig. 17c), and in the city of Tirana with an average speed of 17.4 km/h denoted  $\mathcal{U}_3$  (Fig. 17e). The measurements were performed three times in each scenario.

For the measurement campaign in Austria, a Samsung S8 SM-G950F phone inside the car was connected to the Hutchison Drei 4G (LTE-Advanced) network with carrier aggregation in the downlink. For the measurement campaign in Albania,

a Samsung J600F/DS phone inside the car was connected to the Vodafone Albania 4G (LTE-Advanced) network. For both campaigns, the Android application CDMT [59], developed by Lakeside Labs, was installed on the phone. It recorded various parameters, including the reference signal received power (RSRP), the E-UTRA absolute radio frequency channel number (EARFCN), and GPS coordinates. The EARFCN identifies the carrier frequency the phone is connected to at a given time. Radio measurements for the serving cell along with the neighboring cells were recorded once per second (so  $t \in \mathbb{Z}$  again).

### B. Results

The interference power  $I(t)$  is computed from the measurement traces by adding the RSRP values of all the neighboring cells with the same EARFCN as the serving cell. The interference traces for both the freeway and the urban scenarios are shown in Figs. 16 and 17, respectively. It is evident from the plots that the interference power on the freeway is about one order of magnitude lower than that in the city.

The measured interference is transformed into the binary signal  $J(t)$  based on the threshold  $\theta$  with  $\xi = 0$ . The resulting  $J(t)$  yields the durations  $\tau_{\mathcal{P}}$ ,  $\tau_{\mathcal{V}}$ , and  $\tau$ , which are then analyzed in terms of burstiness, memory coefficient, and burst size, averaged over all measurement campaigns.

The results given in Figs. 18 and 19 and Tables IV and V (for  $\xi = 0$ ) show the following: Burstiness of interference pikes is observed in all scenarios. The pikes tend to be more bursty in the measurements performed in Albania compared to Austria. This could be the result of a denser network deployment to provide coverage to the higher population density in and near Tirana compared to Klagenfurt. Furthermore, in both countries, the freeway scenarios show higher burstiness than the urban scenarios. We conjecture that the higher burstiness on the freeway comes from a combination of the high speed, fast channel variations (caused by the speed), and slow traffic variations (less traffic than in the city). Regarding the memory coefficient, there is no relevant memory present in all measurements. There are only small negative values in Austria and small positive values in Albania. The average interference power is between around  $8 \times 10^{-10}$  mW and  $5 \times 10^{-9}$  mW in all scenarios, where freeway scenarios are more on the lower side of this range. The burst lengths are relatively high with values above 35 s in all scenarios. Further experimental studies need to support these observations and identify the causes of the differences.

## VII. DISCUSSION OF RESULTS

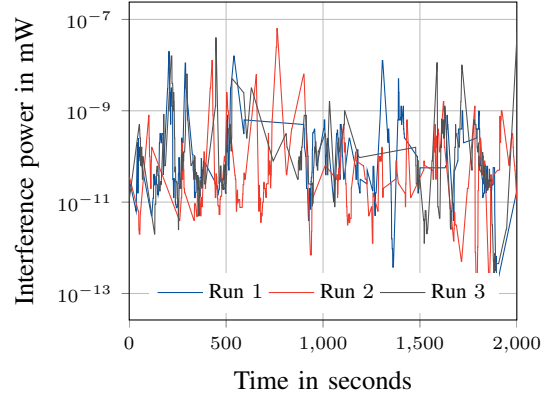
In the synopsis of the model-based and experimental analysis, some insights on the burstiness of interference pikes can be gained. From the model-based analysis, we learn that the burstiness of interference pikes arises from the overlay of fast and slowly changing factors contributing to the overall interference power. For example, in a static network, the burstiness is high when the fast (slowly) changing channel overlays slowly (fast) changing data traffic. Additionally, we observe that the burstiness depends on the type of mobility. For example, the

TABLE III: The effect of different parameters on interference correlation  $\rho$  and burstiness measure  $B$ . Parameters: Mean node speed  $v$ , Nakagami- $m$  parameter, channel block length  $c$  in slots, fraction of transmitting nodes  $\mu$ , and message duration  $d$  in slots. Parameters marked with a dash are irrelevant (an arbitrary positive integer value can be chosen).

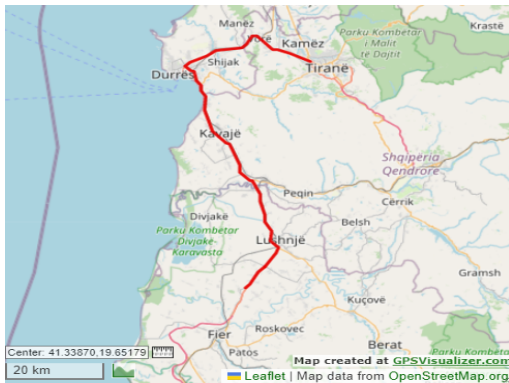
Scenario	Model parameters					Case index [27]			Interference correlation $\rho$	Burstiness measure $B$
	Node $v$	Channel $m$	$c$	Traffic $\mu$	$d$	Node $i$	Channel $j$	Traffic $k$		
$S_1$	$> 0$	$\infty$	–	1	–	2	0	0	Increases with decreasing $v$	Increases with increasing $\rho$
	$> 0$	1	1	1	–		1	0		
	$> 0$	$\infty$	–	$< 1$	1		0	1		
$S_2$	0	1	$> 1$	1	–	0	2	0	Increases with increasing $c$	
	0	1	$> 1$	$< 1$	1	0		1		
$S_3$	0	$\infty$	–	$< 1$	$> 1$	0	0	2	Increases with increasing $d$	
	0	1	1	$< 1$	$> 1$	0	1			
$\mathcal{M}_1$	0	1	$> 1$	$< 1$	$> 1$	0	2	2	Increases with increasing $c$ and $d = 9$	
$\mathcal{M}_2$	$> 0$	1	$> 1$	$< 1$	$> 1$	2	2	2	Increases with decreasing $v$	
Basic	0	1	$> 1$	$< 1$	$> 1$	0	2	2	Increases with increasing $d$ and $c = 15$	



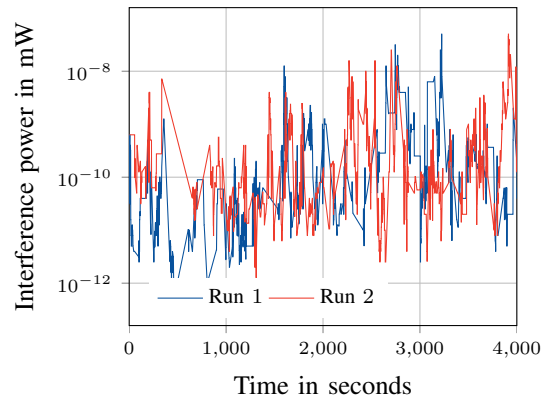
(a) Route (red) for Scenario  $\mathcal{F}_1$ . Length: 73 km.



(b) Measured interference power for Scenario  $\mathcal{F}_1$ .

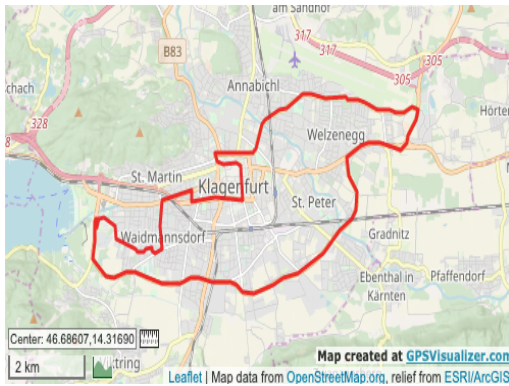
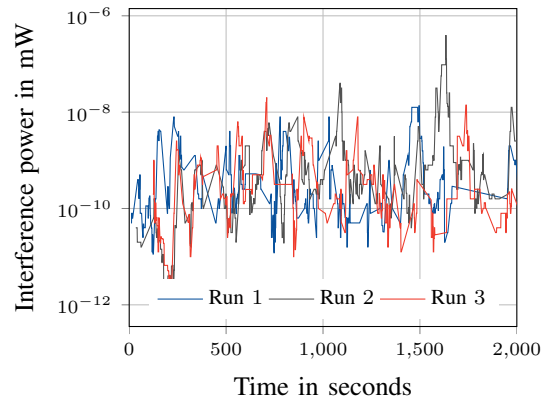


(c) Route (red) for Scenario  $\mathcal{F}_2$ . Length: 94 km.



(d) Measured interference power for Scenario  $\mathcal{F}_2$ .

Fig. 16: Measurement route and measured interference power for freeway scenarios  $\mathcal{F}$  for experimental analysis.


 (a) Route (red) for Scenario  $\mathcal{U}_1$ . Length: 24.6 km.

 (b) Measured interference power for Scenario  $\mathcal{U}_1$ .

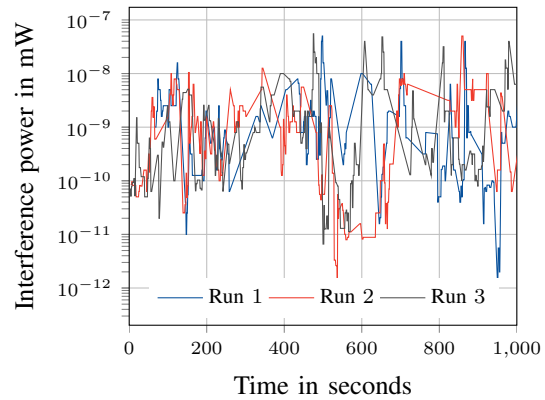
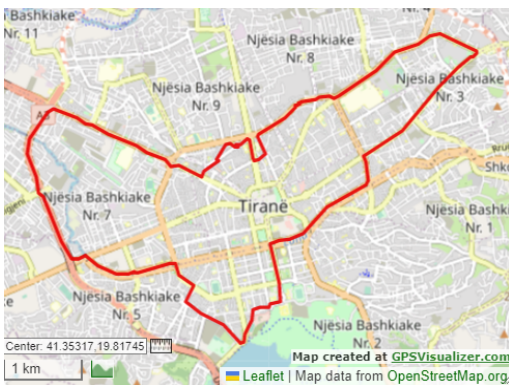
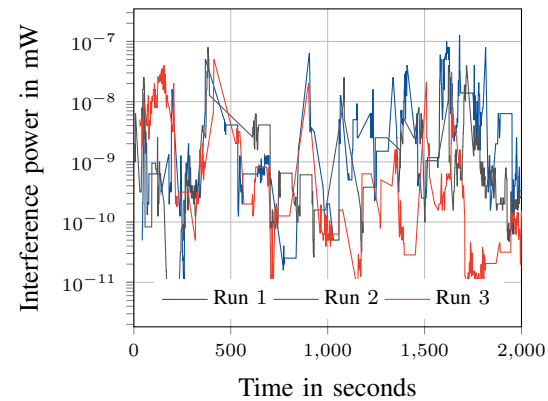
 (c) Route (red) for Scenario  $\mathcal{U}_2$ . Length: 13 km.

 (d) Measured interference power for Scenario  $\mathcal{U}_2$ .

 (e) Route (red) for Scenario  $\mathcal{U}_3$ . Length: 17.5 km.

 (f) Measured interference power for Scenario  $\mathcal{U}_3$ .

 Fig. 17: Measurement route and measured interference power for urban scenarios  $\mathcal{U}$  for experimental analysis.

burstiness is high if interferers follow a Brownian motion as compared to random direction mobility. These insights can be used to design the network with either high or low burstiness of interference pikes, depending on which is preferable for the network. The experimental analysis proves the existence of burstiness of pikes in the real world. However, it is hard to identify the cause of burstiness in experimental data, given how little is known about the interfering nodes in a commercial cellular network. As mentioned, these insights can be exploited for the benefit of the network, e.g., to design opportunistic interference management techniques. Furthermore, given the pikes arrive in bursts, the first pike can be considered a warning

signal for more pikes to come after a relatively short time. This information can be used, e.g., to change the decoding scheme of the receiver, and/or increase the back-off time of the transmitter.

## VIII. CONCLUSIONS AND OUTLOOK

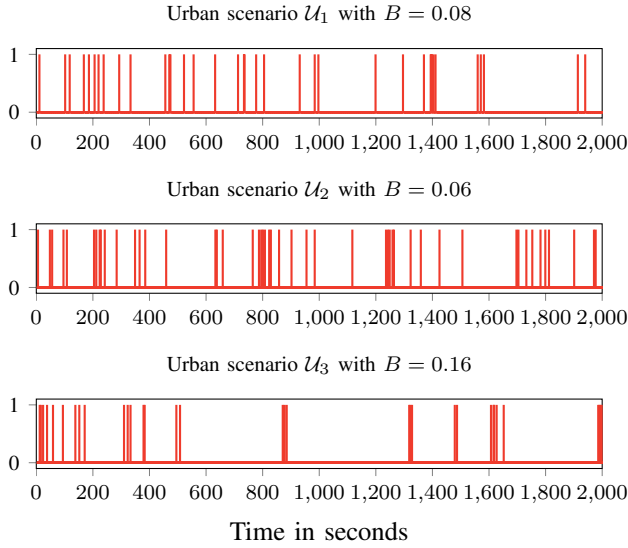
High-interference events in wireless networks can occur in bursts. We analyzed and quantified this phenomenon by simulations and 4G measurements in a variety of scenarios and partly identified its roots. We conjecture that burstiness and memory are fostered by the superposition of rapidly and slowly changing factors contributing to interference.

TABLE IV: Measurement results for the freeway scenario  $\mathcal{F}$  with  $\xi = 0$  and  $\delta = 80$ 

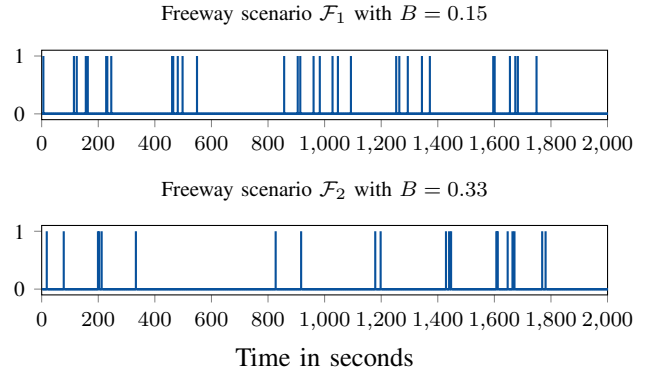
Parameter [unit]	Freeway scenario			
	$\mathcal{F}_1$		$\mathcal{F}_2$	
	mean	std. dev.	mean	std. dev.
$\tau_{\mathcal{P}}$ [s]	5.52	1.91	9.4	1.9
$\tau_{\mathcal{V}}$ [s]	65.84	5.17	48.9	5.4
$\tau$ [s]	71.30	5.04	57.9	7.3
$B$	0.14	0.01	0.336	0.003
$M$	-0.08	0.02	0.048	0.04
$\beta$ [s]	66.6	15.1	49.66	7.15
$I$ [mW]	$2.97 \times 10^{-10}$	$2.25 \times 10^{-09}$	$9.06 \times 10^{-10}$	$3.31 \times 10^{-09}$
No. of pikes per burst	3.09	0.97	3.39	0.62
$\bar{v}$ [km/h]	93		77.2	

 TABLE V: Measurement results for the urban scenario  $\mathcal{U}$  with  $\xi = 0$  and  $\delta = 80$ 

Parameter [unit]	Urban scenario					
	$\mathcal{U}_1$		$\mathcal{U}_2$		$\mathcal{U}_3$	
	mean	std. dev.	mean	std. dev.	mean	std. dev.
$\tau_{\mathcal{P}}$ [s]	8.26	1.03	7.54	1.32	12	4
$\tau_{\mathcal{V}}$ [s]	49.50	14	27.37	2.67	40.8	11.2
$\tau$ [s]	58.32	15	34.92	3.97	52.8	14.9
$B$	0.09	0.03	0.08	0.02	0.219	0.09
$M$	-0.07	0.05	-0.07	0.15	0.067	0.04
$\beta$ [s]	35.3	12.8	138.6	42.6	76.13	14.05
$I$ [mW]	$7.70 \times 10^{-10}$	$4.84 \times 10^{-09}$	$1.60 \times 10^{-09}$	$4.98 \times 10^{-09}$	$4.04 \times 10^{-09}$	$9.53 \times 10^{-09}$
No. of pikes per burst	3.27	1.11	6.85	2.15	4.98	0.55
$\bar{v}$ [km/h]	27		9		17.4	


 Fig. 18: Pike arrivals in a 4G network for urban scenario with  $\xi = 0$ .

We hope that these insights will contribute to a better understanding of interference dynamics, which in turn could be useful in interference management and scheduling. It is expected that future work will include additional measurements and the derivation of analytical results on the stochastic properties of interference pikes.


 Fig. 19: Pike arrivals in a 4G network for freeway scenario with  $\xi = 0$ .

## REFERENCES

- [1] A. Corral, "Long-term clustering, scaling, and universality in the temporal occurrence of earthquakes," *Phys. Rev. Lett.*, vol. 92, no. 10, p. 108501, 2004.
- [2] L. de Arcangelis, C. Godano, E. Lippiello, and M. Nicodemi, "Universality in solar flare and earthquake occurrence," *Phys. Rev. Lett.*, vol. 96, no. 5, p. 051102, 2006.
- [3] M. Wheatland, P. Sturrock, and J. McTiernan, "The waiting-time distribution of solar flare hard x-ray bursts," *The Astrophys. J.*, vol. 509, no. 1, p. 448, 1998.
- [4] T. Kemuriyama, H. Ohta, Y. Sato, S. Maruyama, M. Tandai-Hiruma, K. Kato, and Y. Nishida, "A power-law distribution of inter-spike intervals in renal sympathetic nerve activity in salt-sensitive hypertension-induced chronic heart failure," *Biosystems*, vol. 101, no. 2, pp. 144–147, 2010.

- [5] A.-L. Barabási, “The origin of bursts and heavy tails in human dynamics,” *Nature*, vol. 435, no. 7039, pp. 207–211, 2005.
- [6] J.-P. Eckmann, E. Moses, and D. Sergi, “Entropy of dialogues creates coherent structures in e-mail traffic,” *Proc. of the Nat. Acad. of Sci. (PNAS)*, vol. 101, no. 40, pp. 14333–14337, 2004.
- [7] A. Vázquez, J. G. Oliveira, Z. Dezsó, K.-I. Goh, I. Kondor, and A.-L. Barabási, “Modeling bursts and heavy tails in human dynamics,” *Phys. Rev. E*, vol. 73, no. 3, p. 036127, 2006.
- [8] L. E. Rocha and V. D. Blondel, “Bursts of vertex activation and epidemics in evolving networks,” *PLoS Comput. Biology*, vol. 9, no. 3, 2013.
- [9] V. Paxson and S. Floyd, “Wide area traffic: the failure of Poisson modeling,” *IEEE/ACM Trans. Networking*, vol. 3, no. 3, pp. 226–244, 1995.
- [10] W. E. Leland, M. S. Taqqu, W. Willinger, and D. V. Wilson, “On the self-similar nature of Ethernet traffic (extended version),” *IEEE/ACM Trans. Networking*, vol. 2, no. 1, pp. 1–15, 1994.
- [11] A. Goldsmith, *Wireless Communications*. Cambridge University Press, 2005.
- [12] G. L. Stüber, *Principles of Mobile Communication*. Springer, 4 ed., 2017.
- [13] S. Lin and D. J. Costello, *Error Control Coding*. Prentice Hall, 2 ed., 2001.
- [14] M. K. Atiq, U. Schilcher, and C. Bettstetter, “On interference pikes in Poisson networks,” in *Proc. European Signal Proc. Conf. (EUSIPCO)*, IEEE, 2019.
- [15] R. Vaughan and J. B. Andersen, *Channels, Propagation and Antennas for Mobile Communications*, vol. 50. IET, 2003.
- [16] M. K. Simon and M.-S. Alouini, *Digital Communication over Fading Channels*. John Wiley & Sons, 2005.
- [17] I.-H. Wang, C. Suh, S. Diggavi, and P. Viswanath, “Bursty interference channel with feedback,” in *Proc. IEEE Int. Symp. Inf. Theory (ISIT)*, 2013.
- [18] S. Mishra, I.-H. Wang, and S. N. Diggavi, “Harnessing bursty interference in multicarrier systems with output feedback,” *IEEE Trans. Inf. Theory*, vol. 63, no. 7, pp. 4430–4452, 2017.
- [19] N. Khude, V. Prabhakaran, and P. Viswanath, “Harnessing bursty interference,” in *Proc. Inf. Theory Workshop Netw. and Inf. Theory*, IEEE, 2009.
- [20] S. Kisseleff, J. Kneissl, G. Kilian, and W. H. Gerstaecker, “Efficient detectors for telegram splitting-based transmission in low power wide area networks with bursty interference,” *IEEE Trans. Commun.*, vol. 68, no. 12, pp. 7687–7701, 2020.
- [21] J.-H. Lee, H.-M. Kim, and W. Choi, “Achievable ergodic secrecy rate in bursty interference channels with opportunistic user scheduling,” *IEEE Trans. Commun.*, vol. 67, no. 11, pp. 7686–7699, 2019.
- [22] M. Diamanti, P. Charatsaris, E. E. Tsiropoulou, and S. Papavasiliou, “The prospect of reconfigurable intelligent surfaces in integrated access and backhaul networks,” *IEEE Trans. Green Commun. and Netw.*, vol. 6, no. 2, pp. 859–872, 2022.
- [23] G. Villacrés, T. Koch, A. Sezgin, and G. Vazquez-Vilar, “Robust signaling for bursty interference,” *Entropy*, vol. 20, no. 11, pp. 870–932, 2018.
- [24] R. K. Ganti and M. Haenggi, “Spatial and temporal correlation of the interference in ALOHA ad hoc networks,” *IEEE Commun. Lett.*, vol. 13, no. 9, pp. 631–633, 2009.
- [25] U. Schilcher, S. Toumpis, M. Haenggi, A. Crismani, G. Brandner, and C. Bettstetter, “Interference functionals in Poisson networks,” *IEEE Trans. Inf. Theory*, vol. 62, no. 1, pp. 370–383, 2016.
- [26] U. Schilcher, C. Bettstetter, and G. Brandner, “Temporal correlation of interference in wireless networks with Rayleigh block fading,” *IEEE Trans. Mobile Comput.*, vol. 11, no. 12, pp. 2109–2120, 2012.
- [27] U. Schilcher, J. F. Schmidt, M. K. Atiq, and C. Bettstetter, “Autocorrelation and coherence time of interference in Poisson networks,” *IEEE Trans. Mobile Comput.*, vol. 19, no. 7, pp. 1506–1518, 2020.
- [28] K.-I. Goh and A.-L. Barabási, “Burstiness and memory in complex systems,” *Europhys. Lett.*, vol. 81, no. 4, p. 48002, 2008.
- [29] E.-K. Kim and H.-H. Jo, “Measuring burstiness for finite event sequences,” *Phys. Rev. E*, vol. 94, no. 3, p. 032311, 2016.
- [30] N. Khude, V. Prabhakaran, and P. Viswanath, “Opportunistic interference management,” in *Proc. IEEE Int. Symp. Inf. Theory (ISIT)*, 2009.
- [31] H. Nam, K. S. Ko, I. Bang, and B. C. Jung, “Achievable rate analysis of opportunistic transmission in bursty interference networks,” *IEEE Commun. Lett.*, vol. 22, no. 3, pp. 654–657, 2017.
- [32] S. Kim, I.-H. Wang, and C. Suh, “A relay can increase degrees of freedom in bursty interference networks,” *IEEE Trans. Inf. Theory*, vol. 64, no. 6, pp. 4581–4593, 2018.
- [33] H.-C. Tsao and C. Lin, “Utility maximization for MISO bursty interference channels,” in *Proc. Int. Conf. Wireless Commun. and Signal Process. (WCSP)*, IEEE, 2018.
- [34] U. Schilcher, S. Toumpis, M. Haenggi, A. Crismani, G. Brandner, and C. Bettstetter, “Interference functionals in Poisson networks,” *IEEE Trans. Inform. Theory*, vol. 62, pp. 370–383, Jan. 2016.
- [35] K. Gulati, B. L. Evans, J. G. Andrews, and K. R. Tinsley, “Statistics of co-channel interference in a field of Poisson and Poisson-Poisson clustered interferers,” *IEEE Trans. Signal Process.*, vol. 58, no. 12, pp. 6207–6222, 2010.
- [36] R. W. Heath, M. Kountouris, and T. Bai, “Modeling heterogeneous network interference using poisson point processes,” *IEEE Trans. Signal Process.*, vol. 61, no. 16, pp. 4114–4126, 2013.
- [37] R. K. Ganti and M. Haenggi, “Asymptotics and approximation of the SIR distribution in general cellular networks,” *IEEE Trans. Wireless Commun.*, vol. 15, no. 3, pp. 2130–2143, 2015.
- [38] B. Błaszczyszyn, M. K. Karray, and H. P. Keeler, “Wireless networks appear Poissonian due to strong shadowing,” *IEEE Trans. Wireless Commun.*, vol. 14, no. 8, pp. 4379–4390, 2015.
- [39] T. Camp, J. Boleng, and V. Davies, “A survey of mobility models for ad hoc network research,” *Wireless Commun. and Mobile Comput.*, vol. 2, no. 5, pp. 483–502, 2002.
- [40] E. M. Royer and C. E. Perkins, “Multicast operation of the ad-hoc on-demand distance vector routing protocol,” in *Proc. ACM Int. Conf. Mobile Comput. Netw. (MobiCom)*, 1999.
- [41] Z. Gong and M. Haenggi, “Interference and outage in mobile random networks: Expectation, distribution, and correlation,” *IEEE Trans. Mobile Comput.*, vol. 13, no. 2, pp. 337–349, 2012.
- [42] Z. Gong and M. Haenggi, “Temporal correlation of the interference in mobile random networks,” in *Proc. IEEE Int. Conf. Commun. (ICC)*, 2011.
- [43] P. Nain, D. Towsley, B. Liu, and Z. Liu, “Properties of random direction models,” in *Proc. IEEE INFOCOM*, 2005.
- [44] S. Bandyopadhyay, E. J. Coyle, and T. Falck, “Stochastic properties of mobility models in mobile ad hoc networks,” *IEEE Trans. Mobile Comput.*, vol. 6, no. 11, pp. 1218–1229, 2007.
- [45] S. Kim, J. Cha, S. Jung, C. Yoon, and K. Lim, “Performance evaluation of random access for M2M communication on IEEE 802.16 network,” in *Proc. Int. Conf. Advanced Commun. Technol. (ICACT)*, IEEE, 2012.
- [46] 3GPP TR 37.868, “RAN improvements for machine-type communications,” v. 11.0.0, Oct. 2011.
- [47] P. Zhou, H. Hu, H. Wang, and H.-H. Chen, “An efficient random access scheme for OFDMA systems with implicit message transmission,” *IEEE Trans. Wireless Commun.*, vol. 7, no. 7, pp. 2790–2797, 2008.
- [48] U. Schilcher, J. F. Schmidt, and C. Bettstetter, “On interference dynamics in Matérn networks,” *IEEE Trans. Mobile Comput.*, vol. 19, 2020.
- [49] M. Nakagami, “The  $m$ -distribution — A general formula of intensity distribution of rapid fading,” in *Proc. Symp. Statistical Methods in Radio Wave Propag.*, 1958.

[50] M. Haenggi, *Stochastic Geometry for Wireless Networks*. Cambridge University Press, 2013.

[51] F. Pukelsheim, “The three sigma rule,” *The American Statistician*, vol. 48, no. 2, pp. 88–91, 1994.

[52] H.-H. Jo and T. Hiraoka, “Bursty time series analysis for temporal networks,” in *Temporal Network Theory*, pp. 161–179, Springer, 2019.

[53] M. Karsai, K. Kaski, A.-L. Barabási, and J. Kertész, “Universal features of correlated bursty behaviour,” *Scientific Reports*, vol. 2, p. 397, 2012.

[54] P. Holme and J. Saramäki, “Temporal networks,” *Physics Reports*, vol. 519, no. 3, pp. 97–125, 2012.

[55] M. Karsai, H.-H. Jo, and K. Kaski, *Bursty Human Dynamics*. Springer, 2018.

[56] B.-H. Lee, W.-S. Jung, and H.-H. Jo, “Hierarchical burst model for complex bursty dynamics,” *Phys. Rev. E*, vol. 98, no. 2, p. 022316, 2018.

[57] C. Bettstetter, “Mobility modeling in wireless networks: Categorization, smooth movement, and border effects,” *ACM Mobile Comput. Commun. Rev.*, vol. 5, pp. 55–67, July 2001.

[58] U. Schilcher, C. Bettstetter, and G. Brandner, “Temporal correlation of interference in wireless networks with Rayleigh block fading,” *IEEE Trans. Mobile Comput.*, vol. 11, pp. 2109–2120, Dec. 2012.

[59] C. Raffelsberger, R. Muzaffar, and C. Bettstetter, “A performance evaluation tool for drone communications in 4G cellular networks,” in *Proc. Int. Symp. Wireless Commun. Syst. (ISWCS)*, 2019.



**Mahin K. Atiq** (M’21) received the M.Sc. degree in mobile communications in 2014 from Sejong University in Seoul (South Korea). From 2015 to 2019, she was a research and teaching staff member at the University of Klagenfurt (Austria) with interests in wireless systems and stochastic modeling. She received her Dr.techn. (Ph.D.) degree in information technology in 2021 from the university of Klagenfurt. Her doctoral thesis focused on interference dynamics in wireless networks. Since 2019, she is a researcher at the Silicon Austria Labs (SAL) in Linz, Austria. Her main research interests include wireless networks, stochastic modeling, industrial wireless networks, wireless time-sensitive networking, and 5/6G systems.



**Udo Schilcher** studied applied computing and mathematics at the University of Klagenfurt, where he received two Dipl.-Ing. degrees with distinction (2005, 2006). Since 2005, he was research staff member at the Institute of Networked and Embedded Systems at the University of Klagenfurt. His doctoral thesis on inhomogeneous node distributions and interference correlation in wireless networks and has been awarded with a Dr. techn. degree with distinction in 2011. After his graduation, from 2011 he was Post-Doc, again at the Institute of Networked and Embedded Systems at the University of Klagenfurt. Between 2016 and 2019 he was senior researcher at Lakeside Labs GmbH, where he contributed to projects in the domain of industrial sensor networks. Since 2019, he holds a position as a senior researcher at the University of Klagenfurt. His main interests are interference dynamics, stochastic geometry, IoT, and distributed synchronization algorithms. He received a best paper award from the IEEE Vehicular Technology Society and the IEEE Computer Society.



**Xhemal Pengili** is a senior specialist component verification at Infineon Technologies in Linz, Austria. He studied information and communication engineering at University of Klagenfurt, Austria, where he received the Dipl.-Ing. degree in 2022. He holds a bachelor degree in telecommunication engineering from Polytechnic University of Tirana, Albania.



**Christian Bettstetter** (S'98-M'04-SM'09) received the Dipl.-Ing. degree in 1998 and the Dr.-Ing. degree (summa cum laude) in 2004, both in electrical and information engineering from Technische Universität München (TUM), Munich, Germany. He was a research and teaching staff member at the Institute of Communication Networks, TUM, until 2003. From 2003 to 2005, he was a senior researcher with DOCOMO Euro-Labs. He has been a professor at the University of Klagenfurt, Austria, since 2005, and founding director of the Institute of Networked and Embedded Systems since 2007. He is also the founding scientific director of Lakeside Labs, a research company on self-organizing networked systems.



**Martin Haenggi** (S'95-M'99-SM'04-F'14) received the Dipl.-Ing. (M.Sc.) and Dr.sc.techn. (Ph.D.) degrees in electrical engineering from the Swiss Federal Institute of Technology in Zurich (ETH) in 1995 and 1999, respectively. After a postdoctoral year at the University of California in Berkeley, he joined the University of Notre Dame, IN, USA, in 2001, where he currently is a Professor of electrical engineering and a Concurrent Professor of applied and computational mathematics and statistics. In 2007-2008, he was a visiting professor at the University of

California at San Diego, in 2014-2015 he was an Invited Professor at EPFL, Switzerland, and in 2021-2022, he is a Guest Professor at ETH Zurich. He is a co-author of the monograph "Interference in Large Wireless Networks" (NOW Publishers, 2009) and the author of the textbook "Stochastic Geometry for Wireless Networks" (Cambridge University Press, 2012). His scientific interests include networking and wireless communications, with an emphasis on cellular, amorphous, ad hoc, cognitive, and sensor networks. He served an Associate Editor of the Elsevier Journal of Ad Hoc Networks from 2005-2008, of the IEEE Transactions on Mobile Computing (TMC) from 2008-2011, and of the ACM Transactions on Sensor Networks from 2009-2011, and as a Guest Editor for the IEEE Journal on Selected Areas in Communications in 2008-2009 and the IEEE Transactions on Vehicular Technology in 2012-2013. He also served as a Steering Committee member of the TMC from 2011-2013, as a Distinguished Lecturer for the IEEE Circuits and Systems Society in 2005-2006, as a TPC Co-chair of the Communication Theory Symposium of the 2012 IEEE International Conference on Communications (ICC'12) and of the 2014 International Conference on Wireless Communications and Signal Processing (WCSP'14), as a General Co-chair of the 2009 International Workshop on Spatial Stochastic Models for Wireless Networks (SpaSWiN'09) and the 2012 DIMACS Workshop on Connectivity and Resilience of Large-Scale Networks, and as a Keynote Speaker of SpaSWiN'13, WCSP'14, and the 2014 IEEE Workshop on Heterogeneous and Small Cell Networks. He also served as the Chair of the Executive Editorial Committee (2014-2016) and Editor-in-Chief (2017-2018) of the IEEE Transactions on Wireless Communications. For both his M.Sc. and Ph.D. theses, he was awarded the ETH medal, and he received a CAREER award from the U.S. National Science Foundation in 2005 and three awards from the IEEE Communication society, the 2010 Best Tutorial Paper Award, the 2017 Stephen O. Rice Prize Paper Award, and the 2017 Best Survey Paper Award.